

Identification of brittle/ductile areas in unconventional reservoirs using seismic and microseismic data: Application to the Barnett Shale

Roderick Perez Altamar¹ and Kurt J. Marfurt¹

Abstract

Brittleness in unconventional reservoirs is mainly controlled by mineralogy, and it increases with quartz and dolomite content, whereas an increase in the clay content represents an increase in ductility. To generate regional brittleness maps, we have correlated the mineralogy-based brittleness index to elastic parameters measured from well logs. This correlation can then be used to predict the brittleness from surface seismic elastic parameter estimates of $\lambda\rho$ and $\mu\rho$. We applied the workflow to a 3D seismic survey acquired in an area where more than 400 wells were drilled and hydraulically fractured prior to seismic acquisition. Combining $\lambda\rho$ and $\mu\rho$ into a single 3D volume allowed the combination of both attributes into a single 3D volume, which can be converted to brittleness using a template based on the well log and core data. Neither of these seismic estimates were direct measures of reservoir completion quality. We, therefore, used production logs and extracted surface seismic estimates at microseismic event locations to analyze the completion effectiveness along several horizontal wellbores in the reservoir. We defined four petrotypes in $\lambda\rho$ and $\mu\rho$ space depending on their brittleness and gas saturation, and we found that most of the microseismic events fell into the zone described as brittle in the $\lambda\rho$ - $\mu\rho$ crossplots. These observations supported the well-known idea that regardless of where the well was perforated, microseismic events appeared to preferentially grow toward the more brittle areas, suggesting the growth of hydraulic fractures into the brittle petrotype.

Introduction

The economic success of shale plays depends not only on the formation thickness and the total organic carbon (TOC) content of the reservoir but also on the completion quality. Because of their negligible permeability, almost all shale reservoirs need to be hydraulically fractured. Successful hydraulic fracturing requires targeting the most brittle rocks in which the fractures can be induced, thereby draining the highest amount of gas from the rock.

The study area includes a high-quality 3D seismic survey that was acquired after more than 400 wells had been drilled over a 10-year period using different stimulation fluids (gel, water, and surfactants), and varying numbers of stages, in vertical and horizontal wells.

Poststack seismic attributes, such as coherence and curvature, are routinely used to avoid drilling geohazards, such as faults and karst features, which can connect to nearby water-bearing formations. Although curvature attributes may not illuminate individual fractures, they do quantify the amount of strain (Nelson, 2001). Thompson (2010) and Zhang (2010) show that in the Barnett Shale seismic impedance, curvature, and other attributes can be visually correlated with microseismic events and reservoir performance. Refunjol

et al. (2012) observe that microseismic event locations in the Barnett Shale occurred in areas of low seismic impedance. Rutledge and Phillips (2003) observe a correlation between shear activation of fractures and low seismic impedance.

Perez (2010a, 2010b, 2011) demonstrates that using elastic rock physics parameters, such as Young's modulus E and Poisson's ratio ν or alternatively Lamé parameters λ and μ can characterize a reservoir geomechanically. Most of the engineering literature (e.g., Grieser and Bray, 2007) estimates geomechanical behavior using Young's modulus and Poisson's ratio. Because density is difficult to measure from surface seismic data, Sharma and Chopra (2012) use ρE and ν , resulting in 3D volumetric estimates of geomechanical behavior.

Although hydraulically induced fractures can propagate through ductile and brittle rocks, the goal of the proppant is to better preserve induced fractures in more brittle rocks. Alzate (2012) combines production logs and microseismic data with simultaneous seismic inversion attributes to analyze completion effectiveness along four horizontal wells in the Barnett Shale. He concludes that the hydraulically generated fractures preferentially grow toward the more brittle rock, generating a

¹ConocoPhillips School of Geology and Geophysics, Norman, Oklahoma, USA. E-mail: roderickperezaltamar@gmail.com; kmarfurt@ou.edu. Manuscript received by the Editor 1 March 2013; published online 19 August 2015. This paper appears in *Interpretation*, Vol. 3, No. 4 (November 2015); p. T233–T243, 13 FIGS.

http://dx.doi.org/10.1190/INT-2013-0021.1. © 2015 Society of Exploration Geophysicists and American Association of Petroleum Geologists. All rights reserved.

difference in gas production. Because the 3D seismic survey was acquired after more than 400 wells were drilled and completed in the area, we expect that the findings show evidence of the intensive hydraulic fracturing.

Jarvie et al. (2007) and Wang and Gale (2009) propose brittleness index (BI) definitions based on the mineral composition of the rock, dividing the most brittle minerals by the sum of the constituent minerals in the rock sample, considering quartz (and dolomite, in the case of Wang and Gale, 2009) as the more brittle mineral. However, it is very important to highlight that the term *BI* is a relative measurement that depends on the field of study and the purpose of the investigation (Altindag and Guney, 2010).

The proposed methodology integrates different tools, such as petrophysics, well log analysis, and seismic simultaneous inversion, and it is a continuation of the research done by Perez (2013) and Perez and Marfurt (2014) who described brittle/ductile template based on the mineralogy log measurements and elastic parameters, using the same area of study and data set in the Barnett Shale. The Barnett Shale is well known to be an organically rich and thermally mature formation deposited during Mississippian time in the Fort Worth Basin. It is described to be an unconventional reservoir because of its low average permeability (70 nD) and porosity (6%) distributed in a variety of depositional facies (Deacon, 2011).

Prestack simultaneous inversion was performed to estimate $\lambda\rho$ and $\mu\rho$ seismic volumes in an effort to detect and highlight brittle and ductile regions in an unconventional reservoir. The 2D color bars and interactive 2D crossplotting technology are used to estimate geomechanical behavior from $\lambda\rho$ and $\mu\rho$ estimated from surface seismic inversion. Wells are used with microseismic experiments and surface seismic estimates of $\lambda\rho$ - $\mu\rho$ to quantify damaged rock. At each microseismic location, we extract the corresponding λ and μ values and crossplot the results using a 2D color bar, providing a link between discrete interactive crossplotting and the continuous variability of the data. Finally, we visually correlate anisotropy intensity volumes with microseismic event locations and production wellbore measurements.

Seismic inversion

In an isotropic, linear elastic medium, only two elastic constants (such as Lamé parameters λ and μ) are necessary to completely specify the stress-strain relation. Calibrated by mineralogy logs, these elastic parameters can be used empirically to predict whether a reservoir will deform plastically (for a “ductile” rock) or cataclastically (for a “brittle” rock).

Lamé’s incompressibility parameter λ relates uniaxial and lateral strain to uniaxial stress. The λ is primarily a longitudinal measure and hence “orthogonal” to Lamé’s rigidity parameter μ a quantity that relates shearing stress to strain. Dipole sonic coupled with

P-wave sonic and density logs provide a direct measure of Lamé parameters λ and μ at the well (Goodway, 2007).

Compressional and shear velocities V_P and V_S can be written in terms of Lamé’s parameters λ and μ and bulk density ρ :

$$V_P = \sqrt{(\lambda + 2\mu)/\rho} \quad (1)$$

and

$$V_S = \sqrt{\mu/\rho}. \quad (2)$$

Seismic reflections are sensitive to changes in P- and S-impedances, Z_P and Z_S . We can therefore estimate Lamé impedances (moduli-density relationships) from surface seismic data as follows:

$$\mu\rho = (\rho V_S)^2 = Z_S^2, \quad (3)$$

and

$$\lambda\rho = (\rho V_P)^2 - 2(\rho V_S)^2 = Z_P^2 - 2Z_S^2. \quad (4)$$

Prestack simultaneous inversion estimates P-wave impedance, S-wave impedance, and density, which in turn can be used to predict lithology and geomechanical behavior. Following Goodway et al. (1997) and Goodway (2007), we estimate the P- and S-reflectivities from prestack seismic angle gathers using Fatti et al.’s (1994) method. Then, we estimate P- and S-impedances, Z_P and Z_S , and finally calculate the Lamé impedances $\lambda\rho$ and $\mu\rho$ using equations 3 and 4.

A representative vertical slice (north–south) through $\lambda\rho$ and $\mu\rho$ seismic volumes (Figure 1a and 1b) shows the difference between shale and limestone formations. Limestone formations exhibit a higher $\lambda\rho$ (related to incompressibility) and $\mu\rho$ (related to rigidity) than the shale formations, which show low $\lambda\rho$ and low $\mu\rho$. The Viola Limestone exhibits a higher $\mu\rho$ than the Marble Falls and Forestburg Limestones in the section indicating that it is more rigid than the surrounding shale formations, confirmed by microseismic measurements that show the Viola to be an excellent fracture barrier.

The gamma ray log (Figure 1c) reveals low gamma ray values in the limestone formations, and high gamma ray values in the shale formations. Notice the increase in gamma ray values at the middle of the Lower Barnett Shale formation and its correlation with the decrease in $\lambda\rho$ and $\mu\rho$ (white arrow). We interpret the high gamma ray values to be from an increase in the amount of radioactive minerals (clay). Singh (2008) finds the TOC to be a function of oxygen levels, exhibiting an increase toward the bottom of each parasequence.

To set the template theoretical limits, Perez and Marfurt (2014) compute $\lambda\rho$ and $\mu\rho$ in the three most common minerals in the Barnett Shale: calcite, clay,

and quartz. Connecting the three vertices of each mineral generates a mineralogy ternary plot in $\lambda\rho$ - $\mu\rho$ space.

We crossplot $\lambda\rho$ on the x -axis and $\mu\rho$ on the y -axis, using a 2D color bar with 4096 colors (64×64) to color code the output volume. To be consistent with the previous scale ranges, we set the initial $\lambda\rho$ and $\mu\rho$ axes to range between 0 and 160 $\text{GPa} \cdot \text{g}/\text{cm}^3$ (Figure 2a). However, the 2D histogram shows that the data do not extend through this entire range (Figure 2b); to better use the whole spectrum of colors, we therefore clip the $\lambda\rho$ values from 20 to 100 $\text{GPa} \cdot \text{g}/\text{cm}^3$, and $\mu\rho$ from 10 to 90 $\text{GPa} \cdot \text{g}/\text{cm}^3$ as shown in Figure 3d.

Figure 3a and 3b shows representative slices (east-west) through $\lambda\rho$ and $\mu\rho$ seismic volume, respectively. Figure 3c shows the same vertical slice through cross-plotted $\lambda\rho$ versus $\mu\rho$ seismic volumes using the 2D color bar as shown in Figure 3d. This type of attribute allows the mineralogical discrimination of the reservoir based

on its limestone (magenta, blue, and purple), quartz (yellow and red), and clay (green) content, and therefore its geomechanical behavior.

Figure 4 shows six stratal slices (stratal slice locations are shown in white dashed lines in Figure 3c) through crossplotted $\lambda\rho$ versus $\mu\rho$ seismic volumes corresponding to each formation in this study. Limestone formations, such as Marble Falls Limestone, Forestburg Limestone, and Viola Limestone exhibit magenta, blue, and purple colors, respectively. In contrast, shale formations, such as the Upper Barnett Shale and the Lower Barnett Shale (upper and lower sections) are shown in green, yellow, and red, respectively. This plot enhances the mineralogical composition between the upper and lower section of the Lower Barnett Shale, indicating that the upper section of the Lower Barnett Shale has a higher quartz content than the lower section of the same formation, which exhibits a higher clay content.

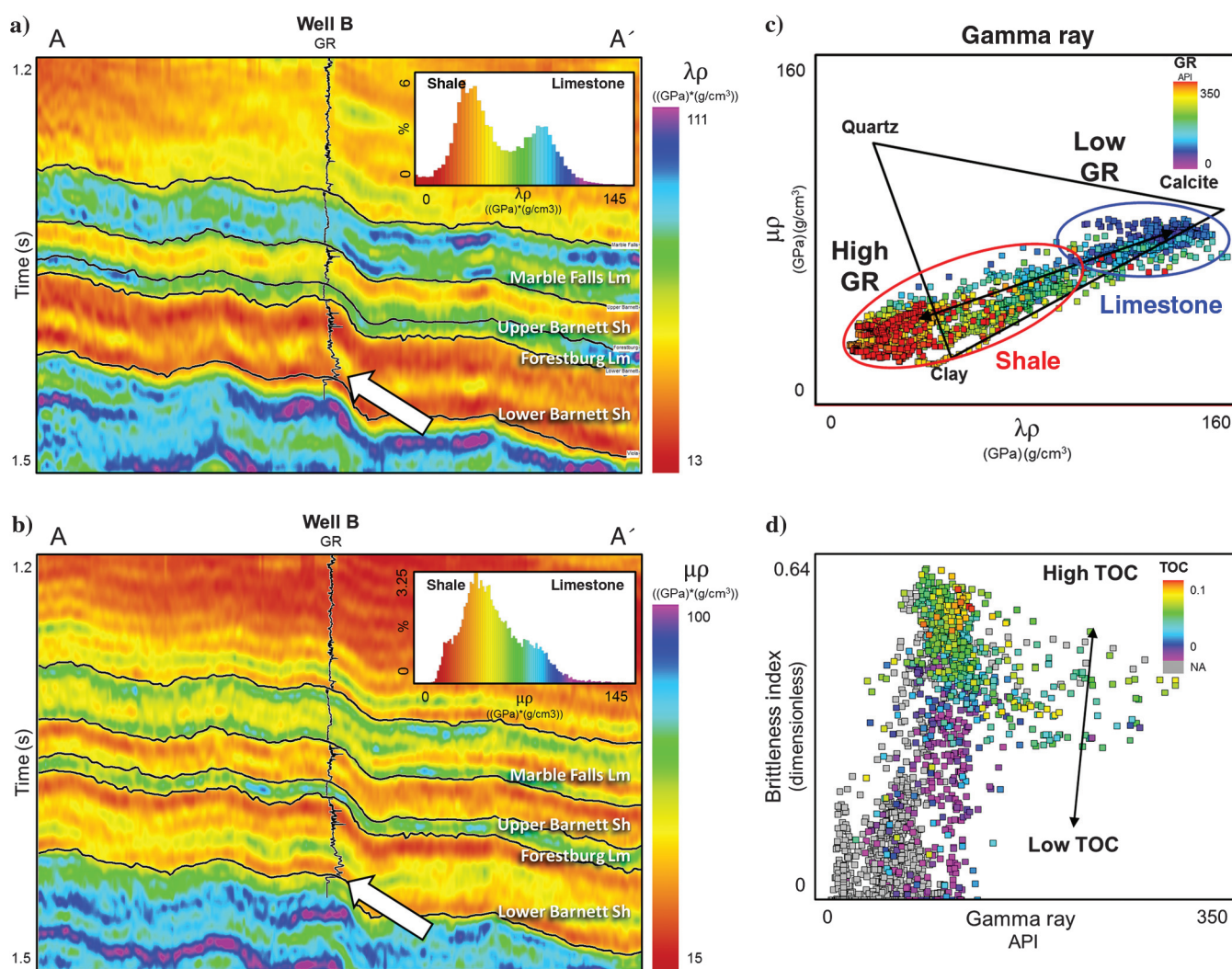


Figure 1. Vertical slices A-A' through (a) $\lambda\rho$ and (b) $\mu\rho$ seismic volumes and their corresponding histograms. Notice that the shale formations exhibit lower values of $\lambda\rho$ and $\mu\rho$ (red and yellow) than the limestone formations (cyan and blue). Location of the line is shown in Figure 4a, and (c) $\lambda\rho$ - $\mu\rho$ crossplot color coded by gamma ray from logs indicating that shale formations exhibit low $\lambda\rho$ and low $\mu\rho$ (Perez and Marfurt, 2014). (d) Gamma ray versus BI indicating that in the Barnett Shale high gamma ray values represent high brittleness and TOC, confirming the core analysis by Singh (2008).

This 2D color bar is a useful tool to interpret geomechanical properties in the reservoir.

We then isolate the $\lambda\rho$ and $\mu\rho$ values corresponding to the Lower Barnett Shale section and generate a specific 2D color bar and histogram displayed in Figure 5a and 5b. This clipped color bar is used to display four

stratal slices corresponding to different layers in the Lower Barnett (Figure 6). Clipping the color bar enhances the horizontal and vertical mineralogy variation of the formation. In the upper section of slice B exhibits a higher quartz content than in the south, and at the same time, slice D exhibits a higher limestone content because it is closer to the Viola Limestone formation. From previous analysis, low $\lambda\rho$ and low $\mu\rho$ indicate less brittle zones, and low $\lambda\rho$ and medium to high $\mu\rho$ indicate more brittle zones. Using the template described in Perez (2013), we use commercial software to generate stratal slices similar to those in Figure 7.

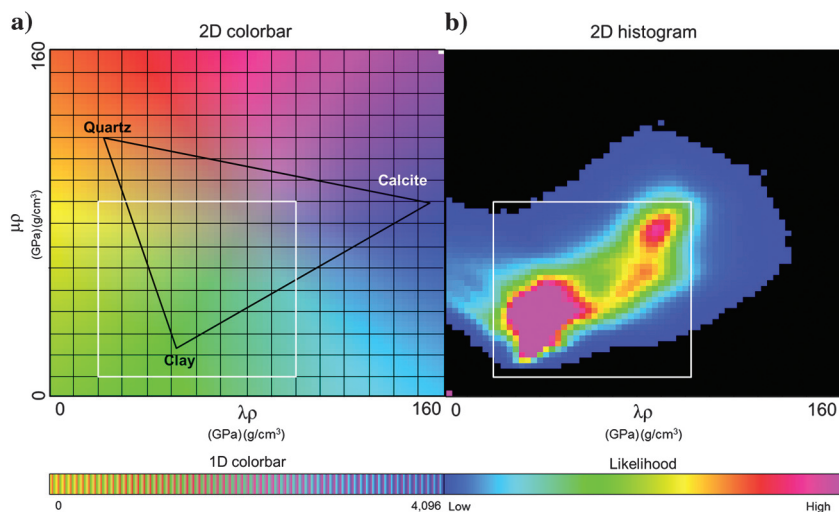


Figure 2. (a) The 2D color bar and its equivalent in 1D, using 4096 (64×64) colors, and (b) 2D histogram corresponding to the $\lambda\rho$ and $\mu\rho$ values from the entire seismic section. The data range is selected to be consistent with figures presented previously. The white rectangle represents the clipped color bar used in Figure 3 to fit all the data.

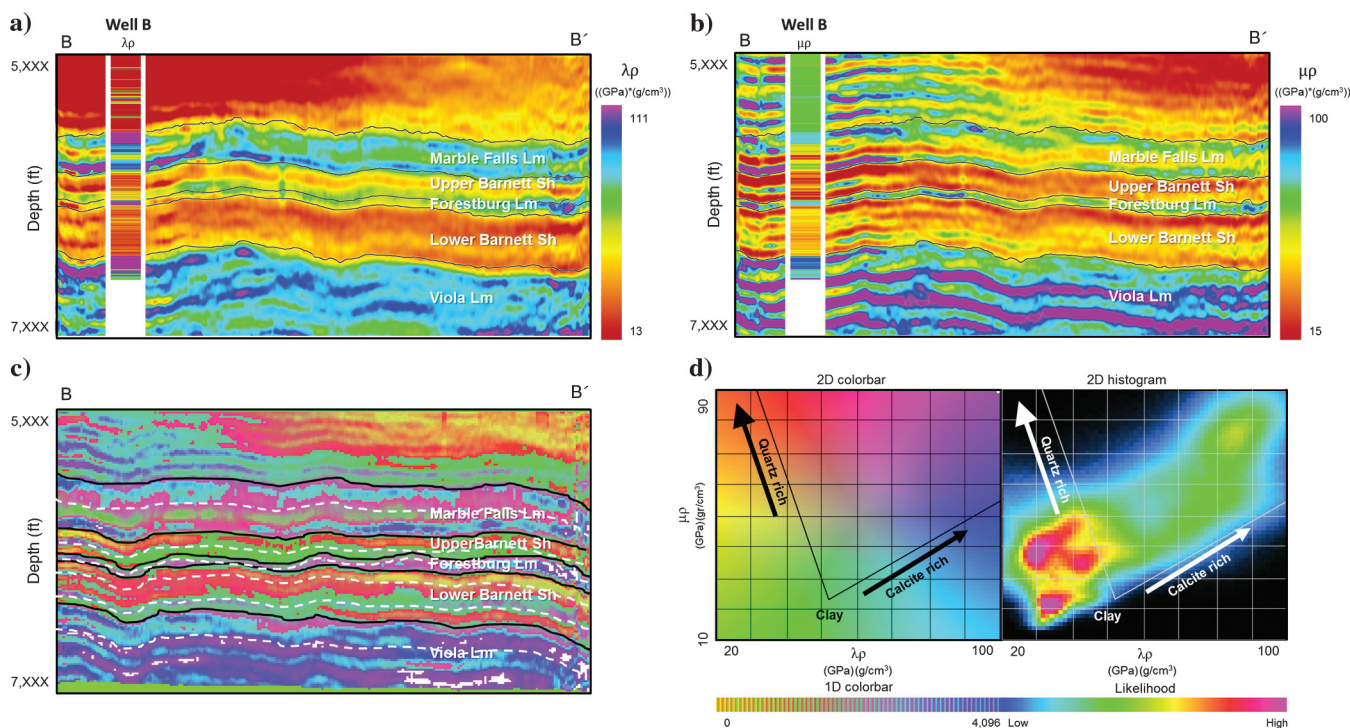


Figure 3. Vertical slices B-B' through (a) $\lambda\rho$ and (b) $\mu\rho$ seismic volumes and (c) through the crossplotted $\lambda\rho$ versus $\mu\rho$ volumes using a (d) 2D color bar. The location of line B-B' is shown in Figure 4a. The range of the 2D color bar enhances the differences between quartz- (yellow and red), clay- (green), and limestone-rich (magenta, blue, and purple) formations, providing an estimate of lithology and geomechanical behavior.

Analysis and discussion Microseismic event analysis

Microseismic monitoring techniques are based on the same principles as earthquake seismology. A complete analysis includes the detection, location, and estimation of magnitude and moments of the microearthquakes induced by hydraulic fracturing and reservoir depletion processes (Warpinski et al., 2005). Microseismic data can be used to evaluate effectiveness of completion designs and map the development of fracture patterns in the reservoir.

During the hydraulic fracturing process, water and any other injected materials (usually sand) are pumped into the wellbore and into the formation through holes that have been perforated through the well-bore casing. The water and other injectables squeeze into the available spaces in the rock until the rock fails. This failure state is reached quicker when the rock is considered brittle (commonly rocks with a high quartz content), resulting in a more effective hydraulic fracture job.

In the Barnett Shale, it is well understood that shear slippage occurs preferably on preexisting planes of weakness as a result of the change in stress and pore pressure that are induced by the fracturing process (Scholz, 1968, 1990). Paleotectonic events in the Fort Worth Basin resulted in a northwest–southeast main stress field orientation. However, the current regional maximum stress direction in the basin is northeast–southwest, with local deviations in intensity and direction due to the presence of the main fault system in the basin, the Mineral Wells–Newark East fault system, and other minor faults. Given this stress regime in the Barnett Shale, we expect that the fractures generated from most of the hydraulic stimulation process are going to have preferred orientation, northeast–southwest.

Eleven wells (nine horizontal and two vertical) with microseismic data are available in the area of study. At the time a fracture occurs S- and P-waves are emitted, which, after processing, provide an estimated position, time, and magnitude of each event (Bennett et al., 2005). Because microseismic data analysis is susceptible to problems associated with sensor placement bias, Alzate (2012) applies several procedures to quality control and filter the microseismic data to avoid issues related to the attenuation of events at large distances.

Most the horizontal wells were drilled along a northwest–southeast azimuth to generate a northeast–southwest-trending fracture pattern, using a different number of stages in each well. Figure 8 shows the direction of four horizontal wells with their microseismic events color coded by stage number. In general, microseismic data show that most of the area around the wellbore was stimulated. However, low activity around the toe of well C indicates that microseis-

mic events are not distributed uniformly along the wellbore.

To validate the previous seismic inversion results, we extract the $\lambda\rho$ and $\mu\rho$ values at each microseismic

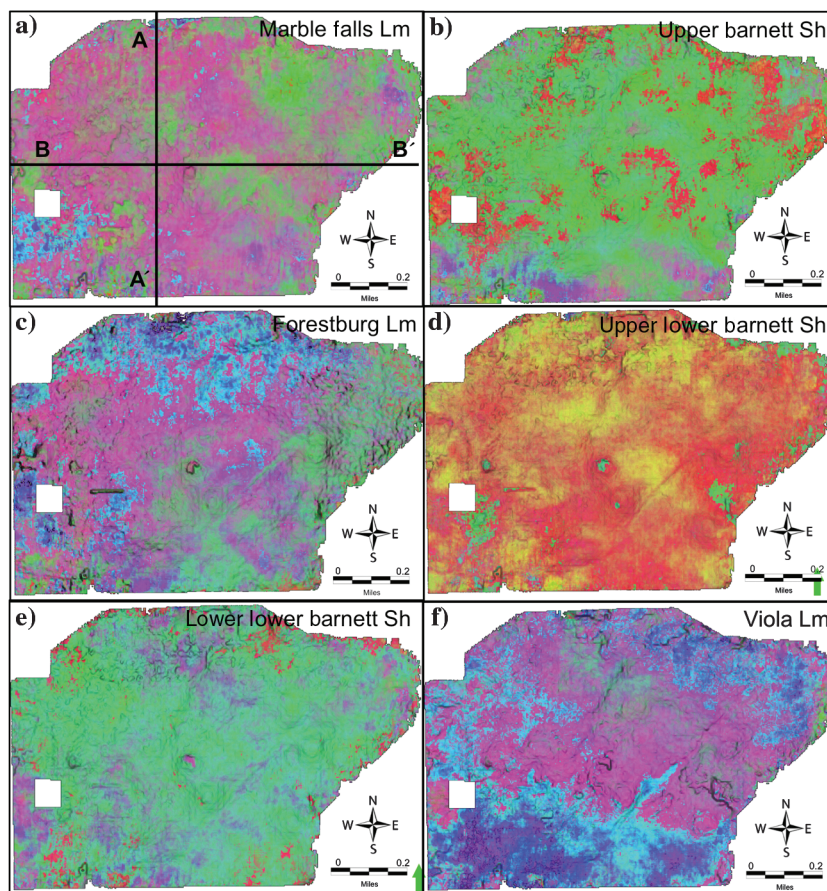


Figure 4. Stratigraphic slices through $\lambda\rho$ versus $\mu\rho$ crossplot volumes corresponding to (a) Marble Falls, (b) Upper Barnett Shale, (c) Forestburg Limestone, (d) upper Lower Barnett Shale, (e) lower Lower Barnett Shale, and (f) Viola Limestone using the 2D color bar indicated in Figure 3d. Stratigraphic slice locations are shown in white in Figure 3c. Limestones appear as magenta, blue, and purple, whereas quartz-rich shales appear as yellow and red, and clay-rich shales appear as green.

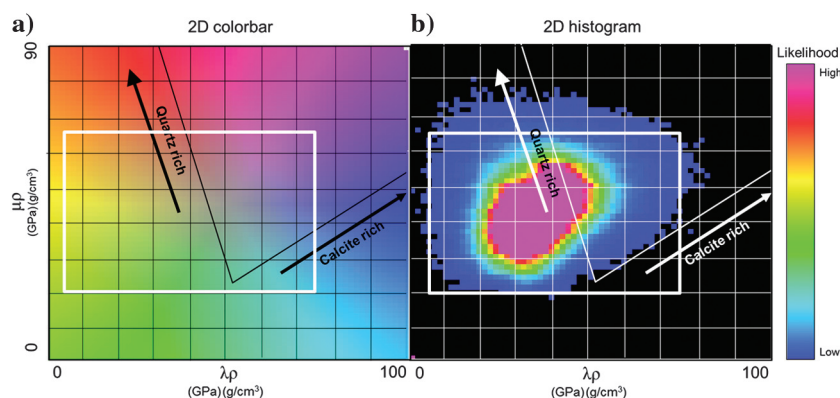


Figure 5. (a) The 2D color bar using 4096 colors and (b) 2D histogram corresponding to $\lambda\rho$ and $\mu\rho$ values from the Lower Barnett Shale section. The white rectangle represents the clipped color bar used in Figures 6, 8, and 11.

event for three wells and display the results in a cross-plot in Figure 9. Then, we calculate a histogram for $\lambda\rho$ and $\mu\rho$ at each stage. In addition, we superimpose in the background $\lambda\rho$ - $\mu\rho$ voxels falling within boxes in Figure 8, and its corresponding histogram in dark gray. Even when the background cloud of voxels is scattered along the plot, a greater population of the microseismic events falls in the zone that we defined as a less brittle zone (orange) and brittle (red).

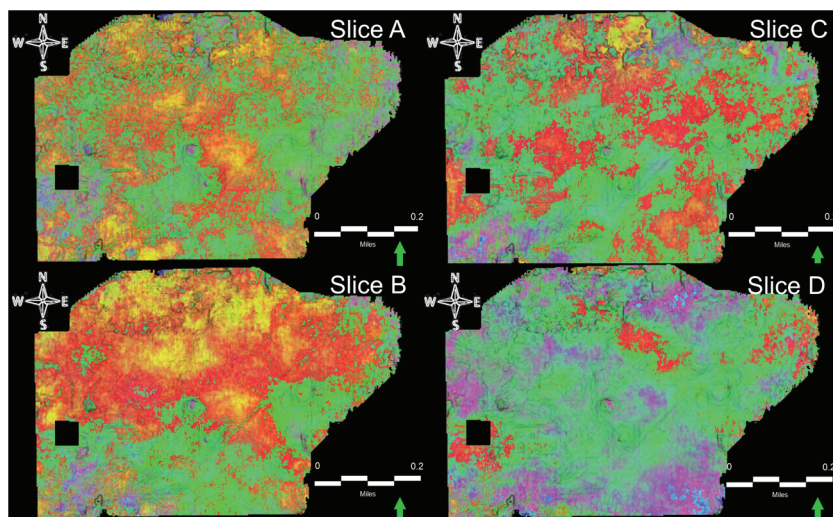


Figure 6. Four stratal slices corresponding to the Lower Barnett Shale indicating the location of the limestone- (magenta and blue), quartz- (yellow and red), and clay-rich shales (green) regions using the 2D color bar as shown in Figure 5a. The location of each slice is shown in Figure 4a.

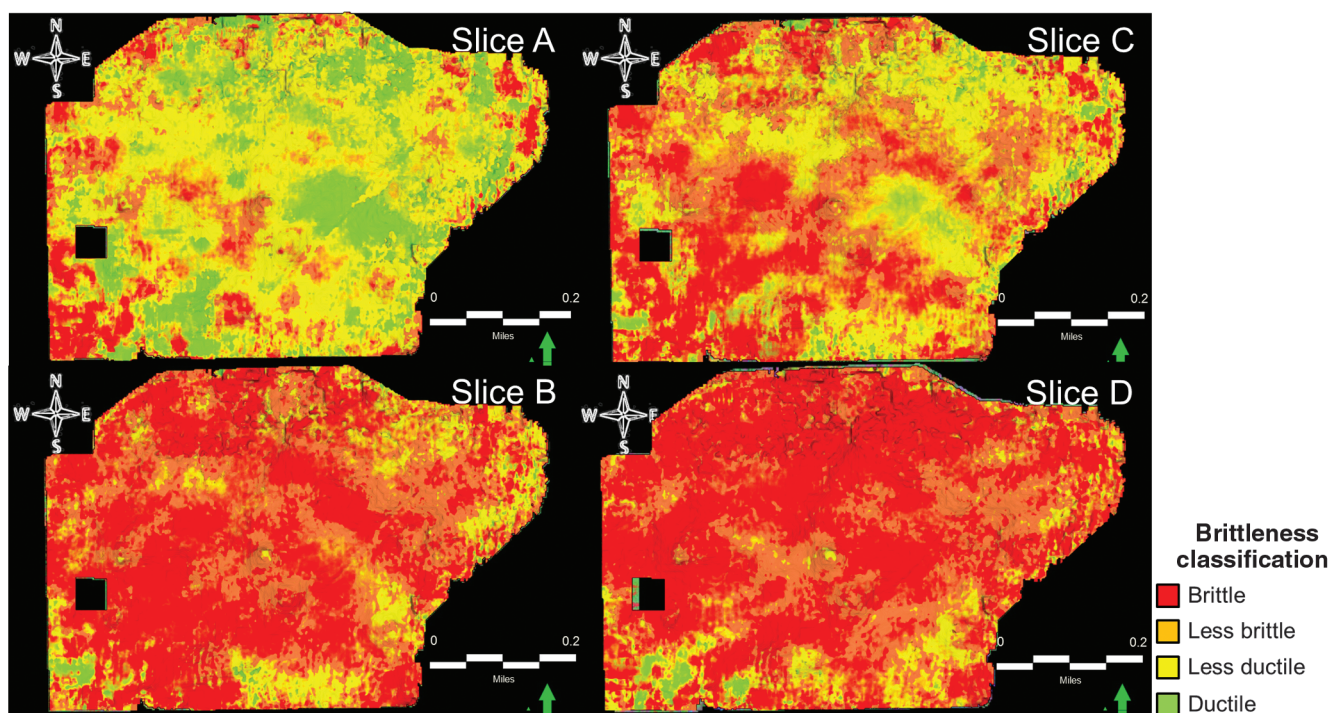


Figure 7. The same four stratal slices presented in Figure 6, corresponding to the lower Barnett Shale indicating the location of the more brittle and less brittle regions using the BI template in the $\lambda\rho$ - $\mu\rho$ space calculated from a well with mineralogy logs 16 mi northeast from the area of study (Figure 12b). Location of each slice is shown in Figure 4a.

Using the same surface seismic data examined in this article, Zhang (2010) calculates the P-wave azimuthal anisotropy intensity and represents microseismic event clouds with polygons, exhibiting a high compartmentalized at the reservoir level, with the compartment edges being defined by structural features (Figure 10). Zhang (2010) calculates the P-wave azimuthal anisotropy using a model based acoustic impedance inversion, which is tightly coupled to the geology by wells, removing most of the seismic wavelet and thin-bed tuning effect. Notice that the microseismic events occur in the low anisotropy zones, which is the opposite of what we expected. These observations suggest that good hydraulic fracturing zones are causing multiple induced fracture orientations in the reservoir. These observations are consistent with the study made by Thompson (2010) in the same area.

These low-anisotropy zones suggest that effective hydraulic fracturing relaxes the rock, thereby locally reducing the anisotropy. Bowker (2007) assumes the Barnett Shale as an overpressured and fully saturated (in terms of sorption) state. Before the reservoir is drilled and hydraulically stimulated, it is at a state of equilibrium, with a balanced pore pressure gradient (3.58 KPa/ft in the gas saturated part of the play) by the

capillary pressure of the rock (Bowker, 2007). When the rock is hydraulically stimulated the equilibrium is disturbed, and gas diffuses from the matrix into the hydraulic fractures, thereby flowing to the wellbore, causing the relaxation of the rock.

We expect that the fractures generated hydraulically create a (local) fracture set perpendicular to the regional reservoir stress field, causing an attenuation in the anisotropy intensity. The change in the fracture geometry caused a change in the anisotropy intensity, in some cases from a vertical transverse isotropic (VTI) symmetry to orthorhombic resulting in a stronger anisotropy signature. However, we assume that after the rock is intensively fractured, it goes from strong horizontal transverse isotropic (HTI) media to orthorhombic exhibiting more isotropy, concluding that the velocity anisotropy is

going to be different due to the fractures generated hydraulically.

Figure 11 shows that the well locations of more 400 wells had already been acquired, and the microseismic events corresponding to zones that had been stimulated (green). This indicates that there are still zones in which there exists the possibility of having bypass pay areas. We observe that the population of microseismic events is higher in the more brittle areas because the fractures propagates to the direction of the less stresses exist and in which they need to do the least amount of work.

Calibration with production logs

Perez et al. (2011) present “heuristic” rock physics templates that can be used to correlate rock composition with $\lambda\rho$ and $\mu\rho$ and production, with the goal of estimating expected ultimate recovery in unconventional reservoirs. Alzate (2012) and Alzate and Devegowda (2013) define four petrofacies, each representing 25% of the data, drawing iso-Poisson’s ratio lines assuming that the variation in the Young’s modulus along these lines is a consequence of the TOC and porosity (Figure 12a). The brittle and rich (red) petrofacies represent areas in the Barnett Shale with low Poisson’s ratio and low Young’s modulus, the ductile and rich (yellow) petrofacies are those regions with high Poisson’s ratio and low Young’s modulus, the brittle and poor (green) petrofacies represent those shales with low Poisson’s ratio and high Young’s modulus, and the ductile and poor (blue) petrofacies are those shales with high Poisson’s ratio and high Young’s modulus.

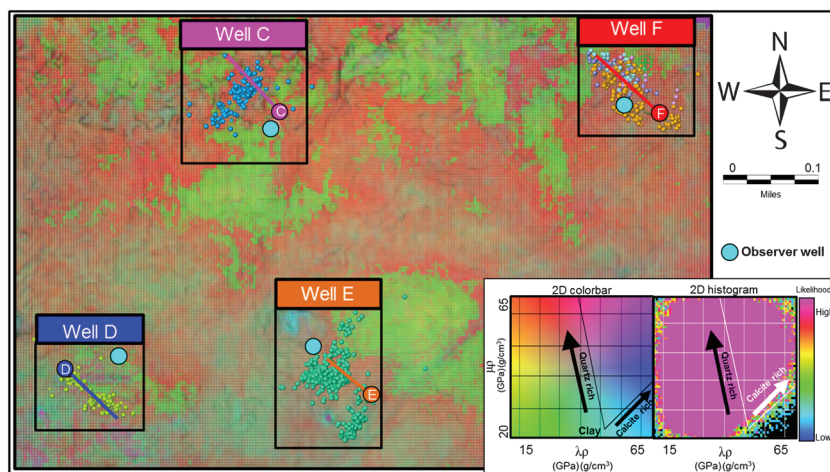


Figure 8. Four microseismic wells (well locations shown in Figure 10) plotted on the top of a stratigraphic slice color coded using the 2D color bar (low right). The red colors represent quartz-rich areas, and therefore they are more brittle than the green areas, which correspond to more ductile zones. Notice that most of the microseismic events are located in the more brittle region, avoiding the ductile zones.

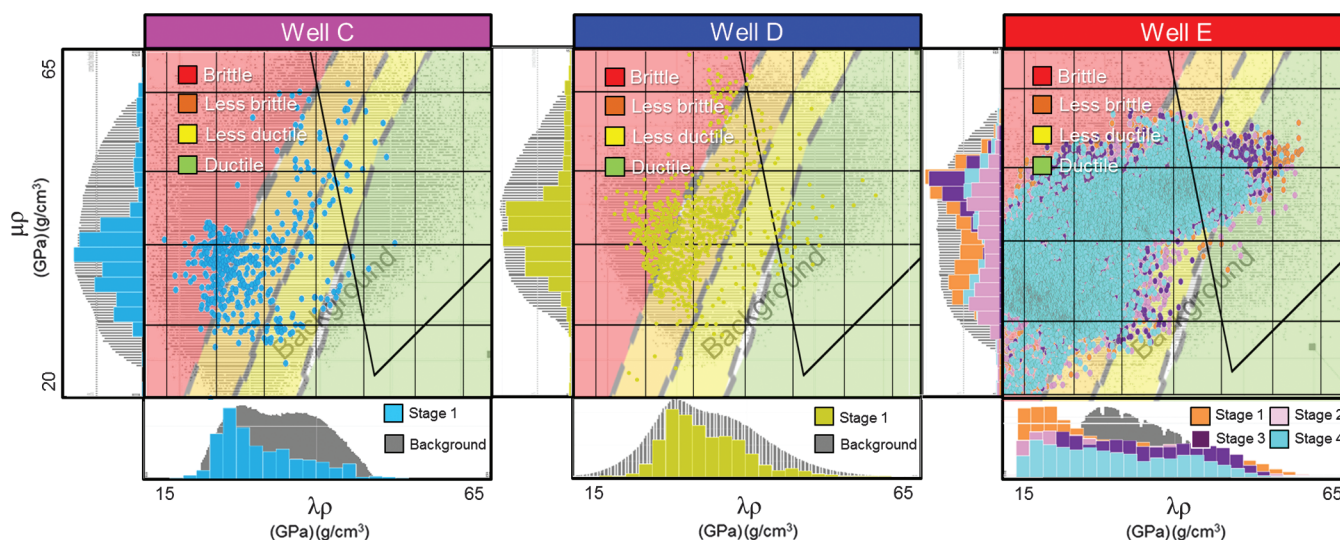


Figure 9. Crossplot in gray of $\lambda\rho$ - $\mu\rho$ of falling voxels within boxes as shown in Figure 8 for the Lower Barnett Shale.

Continuing the work done by [Perez and Marfurt \(2014\)](#), using mineralogy well logs measurements, BI was calculated. Then, we proceed to classify the data population in terms of BI into four petrotypes (brittle, less brittle, less ductile, and ductile).

Brittleness can be defined as the measurement of the stored energy before failure, and it depends on the rock strength, lithology, texture, effective stress, among others parameters. Other brittleness definitions found in the literature were reviewed by [Perez and Marfurt](#)

(2014). At the same time, BI is the ratio between the tensile strength and compressive strength. Because these measurements can only be measured at the laboratory, [Jarvie et al. \(2007\)](#) and [Wang and Gale \(2009\)](#) propose BI definitions based on the mineral composition of the rock. Both authors divide the most brittle minerals by the sum of the constituent minerals in the rock sample, considering quartz (and dolomite, in the case of [Wang and Gale, 2009](#)) as the more brittle minerals.

Using elastic logs, we generate a BI $\lambda\rho\text{-}\mu\rho$ as shown in

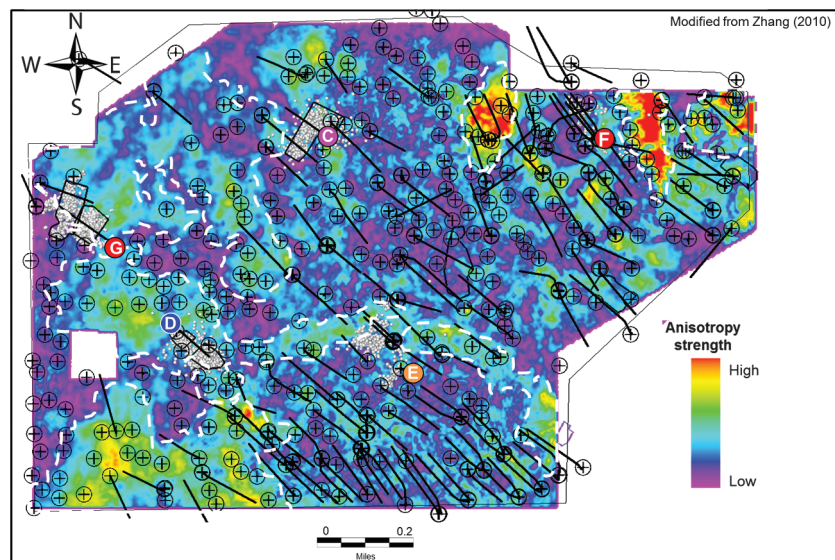


Figure 10. Anisotropy intensity and microseismic event locations from several microseismic events in the Lower Barnett Shale (modified from [Zhang, 2010](#)). Notice that none of the microseismic events occur in areas of high anisotropy. Because 400 additional wells have fractured the rock, we hypothesize that the area of high anisotropy (yellow and red) corresponds to bypassed pay.

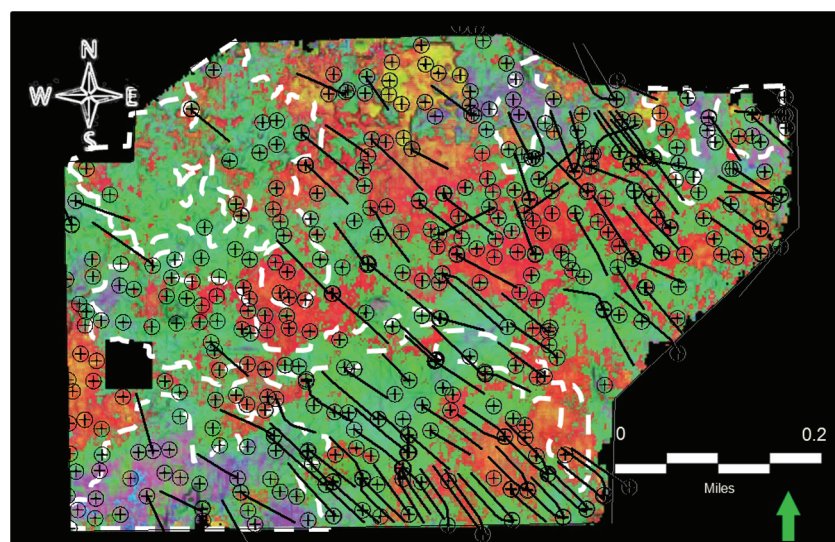


Figure 11. Stratal slice C shown in [Figure 6](#), with the well locations in the area of study using the color bar as shown in [Figure 5](#), in which green represents clay-rich zones, red represents quartz-rich zones, and purple represents calcite-rich zones.

Figure 12b. The rock laboratory measurements are published in Table A-1 by [Mavko et al. \(2009\)](#) (fluid content, dipole logs, and mineralogy logs). Finally, we combine both templates into one ([Figure 12c](#)) agreeing with the [Alzate \(2012\)](#) and [Alzate and Devegowda \(2013\)](#) interpretation. Notice that both independent templates agree in limits in which the data points exist between the iso-Poisson's ratio lines between $\nu = 0.15$ and $\nu = 0.34$. Rock with Poisson's ratio greater than $\nu = 0.23$ is considered brittle, and less than $\nu = 0.23$ is classified as ductile, in which the $\nu = 0.23$ limit was selected as the midpoint between both boundaries ($\nu = 0.15$ and $\nu = 0.34$).

The study area includes four production horizontal wells, which were recorded five months after a multistage hydraulic fracture treatment. Production logs measure flow and provide a quantitative measure of production from each perforation. [Alzate \(2012\)](#) and [Alzate and Devegowda \(2013\)](#) interpret the temperature, differential gas production, and gas and water hold up logs for four wells.

Gas production rates from each perforation are plotted in a $\lambda\rho\text{-}\mu\rho$ crossplot ([Figure 13a](#) and [13b](#)). [Alzate \(2012\)](#) and [Alzate and Devegowda \(2013\)](#) observe that the most prolific zones show low Poisson's ratio and low Young's modulus corresponding to this brittle-rich petrofacies. [Figure 13b](#) shows the well trajectories of the four wells with production logs and how they penetrate different layers, which affects their performance. Based on the microseismic events, [Alzate \(2012\)](#) concludes that no matter in which the well is completed, the fracture will preferentially grow toward the area with the most brittle rock, which explains the difference in gas production between the wells.

Geoscientist community in the oil and gas industry geomechanically clas-

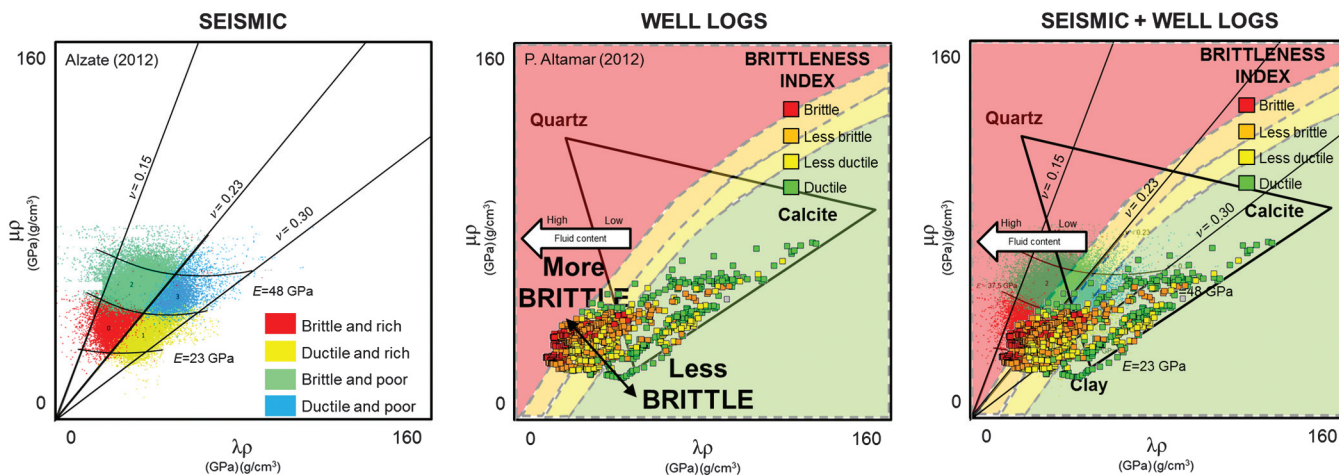


Figure 12. (a) Lower Barnett reservoir quality classification based on the seismically inverted rock properties defining four petrotypes (modified from Alzate, 2012), (b) $\lambda\rho$ versus $\mu\rho$ from well logs (Perez and Marfurt, 2014), and (c) $\lambda\rho$ versus $\mu\rho$ crossplot template after combining panels (a) and (b) classifications. Notice that both templates agree in the region defined as more brittle and with higher fluid content.

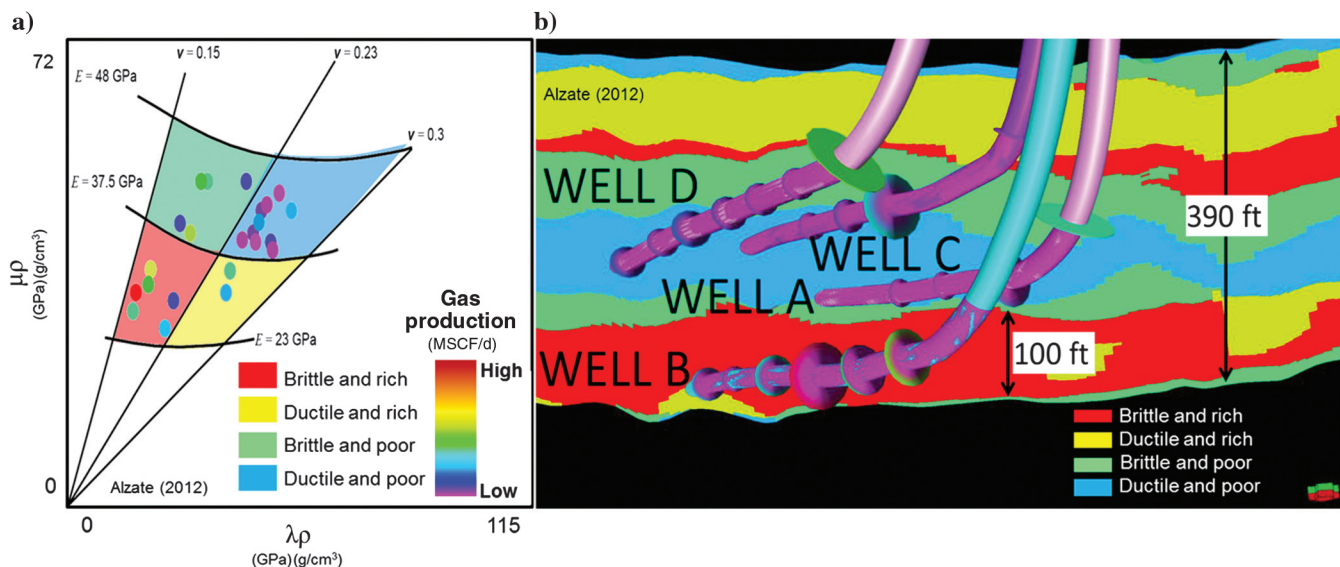


Figure 13. (a) Seismic $\lambda\rho$ - $\mu\rho$ crossplots extracted along the wellbores corresponding to production logs. Each point indicates gas rate at each individual perforation. (b) East-west vertical slides through the reservoir quality volume showing the location of the wells having production logs (modified from Alzate, 2012).

sify a rock in terms of its Poisson's ratio, defining a rock with low and high Poisson's ratio as brittle or ductile rocks, respectively. However, in this specific Barnett Shales case, our results indicates that we need to redefine these concepts calling brittle those rocks with high Poisson's ratio and ductile the rocks with low Poisson's ratio, contrary to the industry wide definitions. Perez and Marfurt (2014) extensively describe the brittleness and BI definitions available in the literature. In this research, we calculate the BI in terms of the mineralogical content of the rock, and not in terms of its geomechanical properties, using Jarvie et al. (2007) and Wang and Gale (2009) 1definitions.

Rocks are fractured at near static conditions (0 Hz) and thus depend on static nonlinear elastic, plastic, and

failure behavior. Surface seismic measurements of elastic properties λ and μ are made between 5 and 150 Hz, whereas those in borehole are made at 10–20 kHz. For this reason, direct seismic estimates of λ and μ are not direct measures of nonlinear behavior. However, through the use of mineralogy logs, Perez (2013) showed that these elastic measurements can be used to predict inelastic behavior.

Conclusions

Simultaneous inversion of surface seismic data not only differentiates shale from limestone but also brittle and ductile shale intervals. The change from brittle to ductile is transitional based on the mineralogy logs and calibrated with microseismic data.

Cutoff from one zone to another is empirical, which is not a serious shortfall in fields with a hundreds of wells. The use of 2D color bars of $\lambda\rho$ versus $\mu\rho$ helps to visualize and quantify the smooth transition between brittle and ductile areas.

Microseismic is an indirect measurement to interpret how the fractures are distributed in the reservoir. We demonstrate that microseismic and production logs show that hydraulically induced fractures preferentially populate brittle regions.

Combining the results of the extracted seismic attributes and measured production logs, we can conclude that more brittle and more fractured the zone is the gas production is higher. Results showing zones in which the anisotropy intensity decreases in areas with high concentration of wells are evidence that the seismic response could be affected after an intense drilling program. In addition, we can conclude that the simultaneous inversion is a very effective tool to discriminate between brittle and ductile zones in unconventional reservoirs.

In this specific case in the Barnett Shale, we are defining as brittle those rocks with high Poisson's ratio and ductile rocks with low Poisson's ratio which is contrary to the industry wide definitions for brittle and ductile rocks, which assume a low Poisson's ratio for brittle and high Poisson's ratio for ductile rocks because the calculated brittleness is based on the rock mineralogical content, and not on its geomechanical properties.

Acknowledgments

We would like to thank Devon Energy for providing the seismic and well data and for the financial support to complete this project, along with Schlumberger (Petrel) and CGG (Hampson-Russell) for providing the software licenses Petrel and Strata to the University of Oklahoma.

Appendix A

Nomenclature

Moduli, densities, and velocities of common minerals.

- λ = Lamé's incompressibility parameter
- μ = Lamé's rigidity parameter
- ρ = Lamé's bulk density parameter
- E = Young's modulus
- ν = Poisson's ratio

References

Altindag, R., and A. Guney, 2010, Predicting the relationships between brittleness and mechanical properties (UCS, TS and SH) of rocks: *Scientific Research and Essays*, **5**, 2107–2118.

Alzate, J. H., 2012, Integration of surface seismic, microseismic, and production logs for shale gas characterization: Methodology and field application: M.S. thesis, The University of Oklahoma.

Alzate, J. H., and D. Devegowda, 2013, Integration of surface seismic, microseismic, and production logs for shale gas characterization: Methodology and field application: *Interpretation*, **1**, no. 2, SB37–SB49, doi: [10.1190/INT-2013-0025.1](https://doi.org/10.1190/INT-2013-0025.1).

Bennett, L., J. LeCalvez, D. R. Sarver, K. Tanner, W. S. Birk, G. Waters, J. Drew, G. Michaud, P. Primiero, L. Eisner, R. Jones, D. Leslie, M. J. Williams, J. Govenlock, R. C. Klem, and K. Tezuka, 2005, The source for hydraulic fracture characterization: *Oilfield Review/Schlumberger*, **17**, 42–57.

Bowker, K. A., 2007, Development of the Barnett Shale Play, Fort Worth Basin: AAPG Search and Discovery Article 10126.

Deacon, R. J., 2011, Barnett provides future returns: *E&P Magazine*, **7175**, 71–75.

Fatti, J., G. Smith, P. Strauss, and P. Levitt, 1994, Detection of gas in sandstone reservoirs using AVO analysis: A 3D seismic case history using the Geostack technique: *Geophysics*, **59**, 1362–1376, doi: [10.1190/1.1443695](https://doi.org/10.1190/1.1443695).

Goodway, B., 2007, A tutorial on AVO and Lamé constants for rock parameterization and fluid detection, http://gsa.seg.org/pdf_forms/RecorderJune2001LMRAVO_new2007july.pdf, accessed 23 January 2013.

Goodway, B., T. Chen, and J. Downton, 1997, Improved AVO fluid detection and lithology discrimination using Lamé parameters $\lambda\rho$, $\mu\rho$ and $\frac{\lambda}{\mu}$ fluid stack from P- and S-inversion: 67th Annual International Meeting, SEG, Expanded Abstracts, 183–186.

Grieser, B., and J. Bray, 2007, Identification of production potential in unconventional reservoirs: Presented at SEP Production and Operations Symposium.

Jarvie, D. M., R. J. Hill, T. E. Ruble, and R. M. Pollastro, 2007, Unconventional shale gas systems: The Mississippian Barnett Shale of North-Central Texas as one model for thermogenic shale-gas assessment: *AAPG Bulletin*, **91**, 475–499, doi: [10.1306/12190606068](https://doi.org/10.1306/12190606068).

Mavko, G., T. Mukerji, and J. Dvorkin, 2009, *The rock physics handbook*: Cambridge University Press.

Nelson, R. A., 2001, *Geologic analysis of naturally fractured reservoirs* 2nd ed.: Gulf Professional Publishing.

Perez, M., D. Close, B. Goodway, and G. Purdue, 2011, Developing templates for integrating quantitative geophysics and hydraulic fracture completions data: Part I — Principles and theory: 81st Annual International Meeting, SEG, Expanded Abstracts, 1794–1798.

Perez, R., 2010a, Determining brittleness in the Barnett Shale using simultaneous impedance inversion: Presented at Student Expo, AAPG-SEG.

Perez, R., 2010b, Application of LMR inversion and clustering analysis in the Barnett Shale: 80th Annual International Meeting, SEG, Expanded Abstracts, 2236–2239.

Perez, R., 2011, Application of LMR and clustering analysis in unconventional reservoirs: Presented at AAPG Geoscience Technology Workshop, International Shale Plays.

Perez, R., 2013, Brittleness estimation from seismic measurements in unconventional reservoirs: Application

- to the Barnett Shale: Ph.D. dissertation, The University of Oklahoma.
- Perez, R., and K. Marfurt, 2014, Mineralogy-based brittleness prediction from surface seismic data: Application to the Barnett Shale: *Interpretation*, **2**, no. 4, T255–T271, doi: [10.1190/INT-2013-0161.1](https://doi.org/10.1190/INT-2013-0161.1).
- Refunjol, X. E., K. M. Keranen, J. H. LeCalvez, and K. J. Marfurt, 2012, Integration of hydraulically induced microseismic events location with active seismic attributes: A North Texas Barnett Shale case of study: *Geophysics*, **77**, no. 3, KS1–KS12, doi: [10.1190/geo2011-0032.1](https://doi.org/10.1190/geo2011-0032.1).
- Rutledge, J. T., and W. S. Phillips, 2003, Hydraulic stimulation of natural fractures as revealed by induced microearthquakes, Carthage Cotton Valley gas field, east Texas: *Geophysics*, **68**, 441–452, doi: [10.1190/1.1567214](https://doi.org/10.1190/1.1567214).
- Scholz, C. H., 1968, Mechanism of creep in brittle rock: *Journal of Geophysical Research*, **73**, 3295–3302, doi: [10.1029/JB073i010p03295](https://doi.org/10.1029/JB073i010p03295).
- Scholz, C. H., 1990, *The mechanics of earthquakes and faulting*: Cambridge University.
- Sharma, R. K., and S. Chopra, 2012, New attribute for determination of lithology and brittleness: 82nd Annual International Meeting, SEG, Expanded Abstracts, doi: [10.1190/segam2012-1389.1](https://doi.org/10.1190/segam2012-1389.1).
- Singh, P., 2008, Lithofacies and sequence stratigraphic framework of the Barnett Shale: Ph.D. dissertation, The University of Oklahoma.
- Thompson, A. M., 2010, Induced fracture detection in the Barnett Shale, Fort Worth Basin, Texas: M.S. thesis, The University of Oklahoma.
- Wang, F. P., and J. F. W. Gale, 2009, Screening criteria for shale-gas systems: *Gulf Coast Association of Geological Societies Transactions*, **59**, 779–793.
- Warpinski, N. R., R. C. Kramm, J. R. Heinze, and C. K. Waltman, 2005, Comparison of single- and dual-array microseismic mapping techniques in the Barnett Shale: Presented at SPE Annual Technical Conference and Exhibition, 95568.
- Zhang, K., 2010, Seismic attribute analysis of unconventional reservoirs, and stratigraphic patterns: Ph.D. dissertation, The University of Oklahoma.



Roderick Perez Altamar received an undergraduate degree (2007) in geophysics engineering from the Universidad Simon Bolivar (Caracas, Venezuela), after spending a year as an exchange student at the University of Oklahoma (OU) during the fall of 2005 to the spring of 2006. He received an M.S. (2008) in geology from OU

under the direction of Roger Slatt, and he received a Ph.D. (2013) in geophysics under the guidance of Kurt Marfurt. He is currently working as a seismic interpretation specialist at Pacific Rubiales in Bogota, Colombia. His dissertation research focuses on seismic attributes applied to reservoir characterization of unconventional reservoirs, with results additionally calibrated with available microseismic data. He has authored several articles with his two advisors, and his dissertation is under review for publication as a book. He has also reviewed several papers for *Interpretation*, among other geoscience magazines. As part of a group effort, he won first place in the 2008 AAPG Imperial Barrel Award (IBA) competition along with his four teammates representing OU. He was also the recipient of the SEG Scholar–Charles C. McBurney Memorial Award 2010–2011, among other scholarships. In addition to his academic duties as a full-time research assistant at OU, he participated and accepted leadership roles in several extracurricular activities on campus, such as president of the OU SEG student chapter (2009–2010), vice president (2007–2008), and secretary (2006–2007) of the Association Friends of Venezuela. He is the IBA Latin America Coordinator for Venezuela, Mexico, and Trinidad and Tobago, and he participates in several committees in AAPG and SEG. He continues to stay informed on advancements in the oil and gas community and always looks forward to learning about new data sets and finding new ways to provide value back to companies with which he collaborates.



Kurt J. Marfurt began his geophysical career teaching geophysics and contributing to an industry-supported consortium on migration, inversion, and scattering (project MIDAS) at Columbia University's Henry Krumb School of Mines in New York City. In 1981, he joined Amoco's Tulsa Research Center and spent the next 18 years doing or leading research efforts in modeling, migration, signal analysis, basin analysis, seismic attribute analysis, reflection tomography, seismic inversion, and multicomponent data analysis. In 1999, he joined the University of Houston as a professor in the Department of Geosciences and as director of Allied Geophysics Laboratories. He is currently a member of the Geophysical Societies of Tulsa and Houston, SEG, EAGE, AAPG, AGU, and SIAM, and he serves as an assistant editor for *GEOPHYSICS*. His current research activity includes prestack imaging, velocity analysis and inversion of converted waves, computer-assisted pattern recognition of geologic features on 3D seismic data, and interpreter-driven seismic processing. His research interests include seismic signal analysis, 3D seismic attributes, seismic velocity analysis, subsurface imaging, and multicomponent data analysis.